Modelling hystereses observed during dwarf nova outbursts

J.-M. Hameury, C. Knigge, J.-P. Lasota, F.-J. Hambsch, R. James

A&A 636, A1 (2020)
https://doi.org/10.1051/0004-6361/202037631

Astronomy & Astrophysics

Modelling hystereses observed during dwarf nova outbursts

J.-M. Hameury[1], C. Knigge[2], J.-P. Lasota[3,4], F.-J. Hambsch[5,6,7], and R. James[7]

[1] Observatoire Astronomique de Strasbourg, Université de Strasbourg, CNRS UMR 7550, 67000 Strasbourg, France
e-mail: jean-marie.hameury@astro.unistra.fr
[2] School of Physics and Astronomy, University of Southampton, Southampton SO17 1BJ, UK
[3] Institut d'Astrophysique de Paris, CNRS et Sorbonne Universités, UPMC Paris 06, UMR 7095, 98bis Bd Arago, 75014 Paris, France
[4] Nicolaus Copernicus Astronomical Center, Polish Academy of Sciences, Bartycka 18, 00-716 Warsaw, Poland
[5] Vereniging Voor Sterrenkunde (VVS), Oostmeers 122 C, 8000 Brugge, Belgium
[6] Bundesdeutsche Arbeitsgemeinschaft für Veränderliche Sterne e.V. (BAV), Munsterdamm 90, 12169 Berlin, Germany
[7] American Association of Variable Star Observers, 49 Bay State Road, Cambridge, MA 02138, USA

Received 31 January 2020 / Accepted 6 March 2020

ABSTRACT

Context. Although the disc instability model is widely accepted as the explanation for dwarf nova outbursts, it is still necessary to compare its predictions to observations because many of the constraints on angular momentum transport in accretion discs are derived from the application of this model to real systems.
Aims. We test the predictions of the model concerning the multicolour time evolution of outbursts for two well-observed systems, SS Cyg and VW Hyi.
Methods. We calculate the multicolour evolution of dwarf nova outbursts using the disc instability model and taking into account the contribution from the irradiated secondary, the white dwarf and the hot spot.
Results. Observations definitely show the existence of a hysteresis in the optical colour–magnitude diagram during the evolution of dwarf nova outbursts. We find that the disc instability model naturally explains the existence and the orientation of this hysteresis. For the specific cases of SS Cyg and VW Hyi, the colour and magnitude ranges covered during the evolution of the system are in reasonable agreement with observations. However, the observed colours are bluer than observed near the peak of the outbursts, as in steady systems, and the amplitude of the hysteresis cycle is smaller than observed. The predicted colours significantly depend on the assumptions made for calculating the disc spectrum during rise, and on the magnitude of the secondary irradiation for the decaying part of the outburst.
Conclusions. Improvements in the spectral disc models are strongly needed if the system evolution in the UV is to be addressed.

Key words. accretion, accretion disks – stars: dwarf novae – instabilities

1. Introduction

Dwarf novae are a subclass of cataclysmic variables that undergo regular 4–6 mag outbursts lasting from one to a few days, with a typical recurrence time of a few weeks (see Warner 2003, for a review). It is now widely accepted that these outbursts are caused by a thermal-viscous instability of the accretion disc that occurs when the disc temperature is of the order of the ionisation temperature of hydrogen, and the opacities become strongly temperature-dependent (see Lasota 2001; Hameury 2019, for reviews of the model).

Although the disc instability model (DIM) is based on the assumption that angular momentum transport in the disc can be described by an effective viscosity depending on a single parameter (Shakura & Sunyaev 1973), the DIM has been quite successful in explaining the overall properties of dwarf nova outbursts. We know now, however, that the assumption that energy dissipation is local and is due to the transport of angular momentum, and that it can be described by the Shakura–Sunyaev viscosity, is at best very crude. The magnetorotational instability (MRI) is most probably responsible for angular momentum transport during bright states (Balbus & Hawley 1991), when the disc is hot and fully ionised, but the situation could be quite different during the quiescence (see e.g. Coleman et al. 2016; Scepi et al. 2018). Progress in our understanding of angular momentum transport in accretion discs will come from theoretical studies of the various physical processes that might be involved and also from a comparison of the predictions of the DIM with observations.

The DIM nicely reproduces the timing properties of dwarf nova outbursts, but the wealth of observations extends well beyond light curves. Eclipse mapping provides the brightness variations along the disc radius (Horne 1985), and hence the radial dependence of the effective temperature that can be directly compared to models. Observational results do not always seem to agree well with predictions from the DIM: in the case of EX Dra, the quiescent temperatures are too high, and their radial distribution corresponds to that of a steady disc (Baptista 2016), in particular in the inner disc. It is unclear whether this is a deficiency of the DIM or if it is due to systematic effects generated by the high inclination of eclipsing systems (85° in the case of EX Dra; see Smak 1994, for high inclination effects on the temperature profiles). In other systems with lower inclinations, such as Z Cha (Horne & Cook 1985), the agreement is better. Spectral fitting is not restricted to systems that are almost edge-on, but it deals with the difficulty that models,

even sophisticated ones that take into account effects such as variations in the vertical component of gravity with altitude or viscous heat dissipation in the disc atmosphere (Hubeny 1990), do not reproduce well the observed spectra of novalike systems, in particular in the UV (see Nixon & Pringle 2019 for a recent discussion of this problem and Wade 1988, 1984; Knigge et al. 1997, 1998; Yi & Kenyon 1997; Puebla et al. 2007 for a historical perspective). Fitting the details of time-dependent spectra is then unlikely to provide much information on dwarf novae; this conclusion is reinforced by the fact that our understanding of the spectra in the low state is very poor, despite some efforts in the past years (Idan et al. 2010).

For these reasons, and despite an early work by Cannizzo & Kenyon (1987), comparisons with observations have been limited to colour, and notably to the so-called UV delay at a time when it was believed that the time-lag between the rise in the UV and in the optical was an indicator of the inside-out (the outburst is triggered in the inner part of the disc) or outside-in nature of the dwarf nova eruption. Schreiber et al. (2003) showed that this was not the case, because a significant increase in the UV requires that the mass accretion rate at the inner disc edge also increases by a large fraction, which takes longer than the propagation time of the heating front, which occurs in a fraction of the viscous time estimated in the inner parts of the disc.

In this paper we calculate the colour variations in B and V that are predicted by the DIM and compare them to observations; we also briefly discuss the situation in the ultraviolet (U band). We improve on the early work by Cannizzo & Kenyon (1987) by using a more elaborate version of the DIM that solves the full vertical structure of discs, has sufficient spatial resolution to resolve the structure of heat fronts, and allows for variations in the outer disc radius, which has a profound influence on the outburst cycle (Hameury et al. 1998), in particular on the occurrence of outside-in versus inside-out outbursts. Cannizzo & Kenyon (1987) assumed that matter was added to the disc at the circularisation radius, that is the radius at which matter leaving the L_1 point would form circular orbits while keeping its initial angular momentum; we assume here that it is added at the outer disc edge. We also take into account the contribution of the secondary star and of the hot spot, which can be very significant in particular for long orbital period systems. We finally account for the specific parameters of the observed systems. On the negative side, we use a simplified treatment of the disc spectral properties by not taking into account the energy dissipation in the photosphere when estimating the flux emitted at different spectral bands.

It has long been known that in the colour–colour ($U - B$, $B - V$) plane a dwarf nova such as VW Hyi follows a loop (Bailey 1980). This hysteresis-type behaviour is similar to that found when considering variations of the optical flux versus the X-ray to extreme ultraviolet (EUV) plus X-ray flux in SS Cyg (Hameury et al. 2017) and, as we discuss below, is accounted for by the same effect: a complete change in the disc's mass distribution during outburst. Soft X-ray transients (SXTs), which are the analogues of dwarf novae in low-mass X-ray binaries, also exhibit a hysteresis in the hardness-intensity diagram, but despite apparent similarities with the hysteresis found in dwarf novae (Körding et al. 2008) its origin is different and unrelated to the DIM (Hameury et al. 2017); for SXTs the viscous timescale in the X-ray emitting regions is much shorter than the outburst duration, and the DIM does not predict any difference between the X-ray properties of the rise and decay of disc outbursts.

In Sect. 2 we present the available observations in the visible for SS Cyg and VW Hyi from the American association of variable star observers (AAVSO) and in particular the time evolution in a colour–magnitude diagram that extends Bailey (1980) observations to the visible band and are easier to interpret; in Sect. 3 we describe our methods and assumptions for estimating the integrated colours; and we present out results together with the comparison with observations both from the AAVSO and from Bailey (1980) in Sect. 4. The objective here is not to fit precisely the observational data, given the uncertainties and approximations inherent to the DIM, but rather to check if the general characteristics of the observations can be accounted for by the DIM.

2. Observational data

SS Cyg has an orbital period of 6.60 h; it is one of the best observed dwarf novae, with an extended historical coverage by the AAVSO beginning at the end of the 19th century. We selected two well-covered consecutive outbursts with available data in the B and V bands, with reasonable error bars, obtained by the same observer (Roberts 2019); the B magnitude is obtained in most cases 20 min earlier than the V magnitude. The first outburst was triggered on August 9, 2012, and lasted for slightly more than two weeks; the second started on October 25, 2012 (i.e. 76 days later), and also lasted for two weeks. Figure 1 shows the light curve of these two outbursts. The SS Cyg outburst distribution is bimodal, and consists of long (two weeks) and bright outbursts and a roughly equal number of short (one week) and slightly fainter ones (Bath & van Paradijs 1983); the outbursts we selected fall into the first category; in addition there is a doubled-peak light curve for the second outburst, which is relatively rare but not exceptional. The observed colour–magnitude diagram is shown in Fig. 2. The statistical uncertainties on $B - V$ are typically around 0.03 mag. Systematic errors may be larger, but should be less than 0.1 mag, although there could be some colour dependence present. The systematics may, however, be different for bright ($V < 11$) and faint ($V > 11$) phases, due to the use of different comparison stars. In quiescence, $B - V$ is approximately 0.7; SS Cyg becomes bluer in outburst, with a $B - V$ reaching 0.35. This is not unexpected, but what is more remarkable is that the colours during the rise and the decay are significantly different, the rise being redder than the decay.

We then consider the case of VW Hyi, which is a source that has been well observed by amateur astronomers, and we selected two consecutive outbursts from the AAVSO database that occurred on September 7 and October 2, 2018 (Hambsch 2019); these are shown in Fig. 3. As can be seen, these two outbursts have remarkably similar shapes. VW Hyi has an orbital period of 1.78 h, and is the brightest and the best observed system belonging to the SU UMa subclass that presents, in addition to normal outbursts, brighter and much longer superoutbursts. It is generally believed that superoutbursts are caused by a tidal instability coupled to the thermal-viscous instability (Osaki 1989), but the validity of this model has been questioned by Buat-Ménard & Hameury (2002), Smak (2009), and Cannizzo (2012) who favoured a model based on irradiation-enhanced mass transfer from the secondary (Hameury et al. 2000). Whatever the mechanism accounting for superoutbursts, the two bursts we selected belong to the category of normal outbursts, and are caused by the classical thermal-viscous instability.

The colour–magnitude diagram of VW Hyi is shown in Fig. 4. As for SS Cyg, the statistical uncertainties on $B - V$ are typically around 0.03 mag., and the systematic errors less than

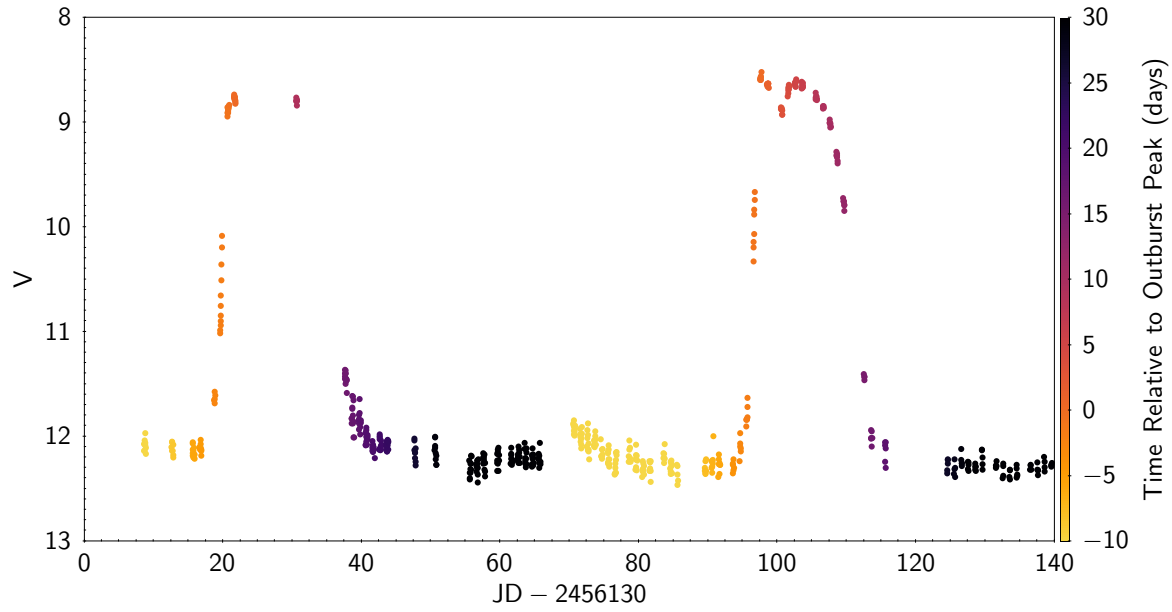

Fig. 1. SS Cyg light curve from the AAVSO in the *V* band.

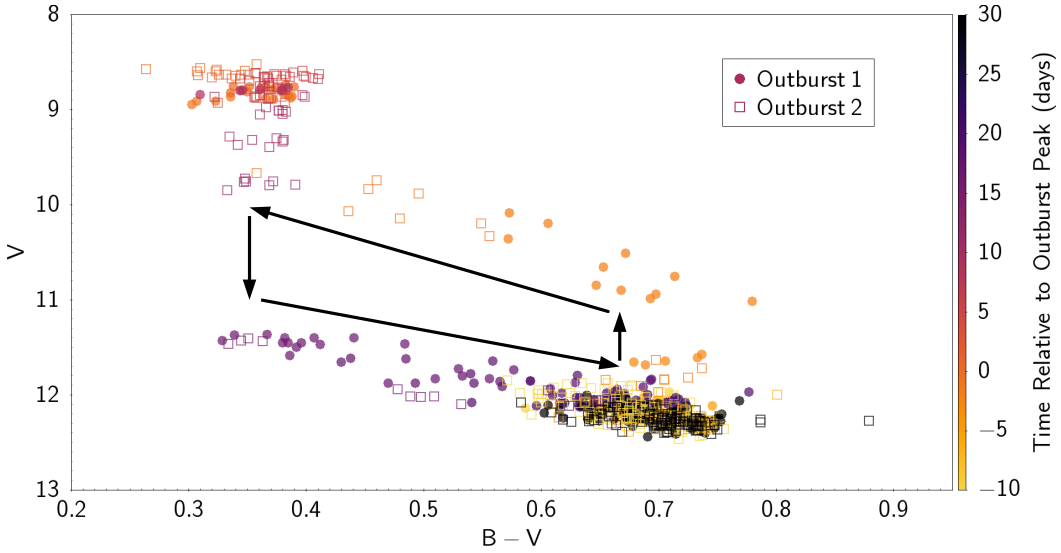

Fig. 2. Colour variations across two outbursts of SS Cyg. The colour-coding is the same as in Fig. 1, and represents the time. The arrows show the direction of the time evolution in the diagram.

0.1 mag., with no difference between bright and faint states due to the use of the same comparison stars. This diagram is very similar to that of SS Cyg, the main difference being that VW Hyi is bluer both in quiescence and in outburst, and that during the initial rise the system becomes redder by almost half a magnitude. In both cases, a hysteresis is clearly visible with an amplitude similar to that of SS Cyg.

These results are, as far as the *B* and *V* magnitudes are concerned, comparable to those of Bailey (1980); our colours at a given magnitude are similar to his, and he also finds that during the rise of VW Hyi, the system first reddens before becoming bluer. A comparison of both sets of observations during decay is unfortunately impossible since he did not provide the optical magnitudes during decay in his Figs. 1 and 2.

It therefore appears that both systems are, for a given optical magnitude, bluer during decay than during rise by about 0.2−0.4 mag, and that the decay occurs at a roughly constant $B - V$. SS Cyg becomes bluer during the rise, while VW Hyi initially reddens before evolving in a similar way to SS Cyg. These are the main characteristics that, to be successful, the DIM should be able to reproduce.

3. Model

In order to model the light curve in various bands we include the contributions from the accretion disc, the secondary star, the hot spot, and the white dwarf, following the method described in Schreiber et al. (2003), which we briefly summarise here. The contribution from the boundary layer, even in the *U* band, is negligible compared to the disc and white dwarf contribution and, although it has been included, is not described here (see Schreiber et al. 2003 for more details).

3.1. Disc contribution

We use the code described in Hameury et al. (1998) for the DIM. As we consider the hot spot to be a separate source of

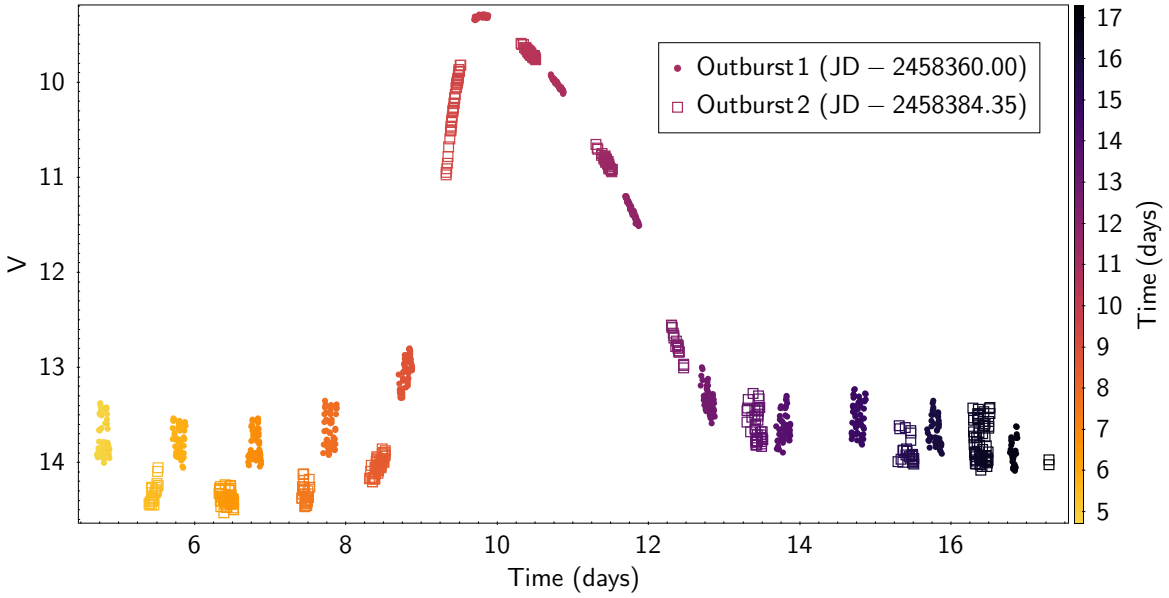

Fig. 3. VW Hyi light curve from the AAVSO in the *V* band.

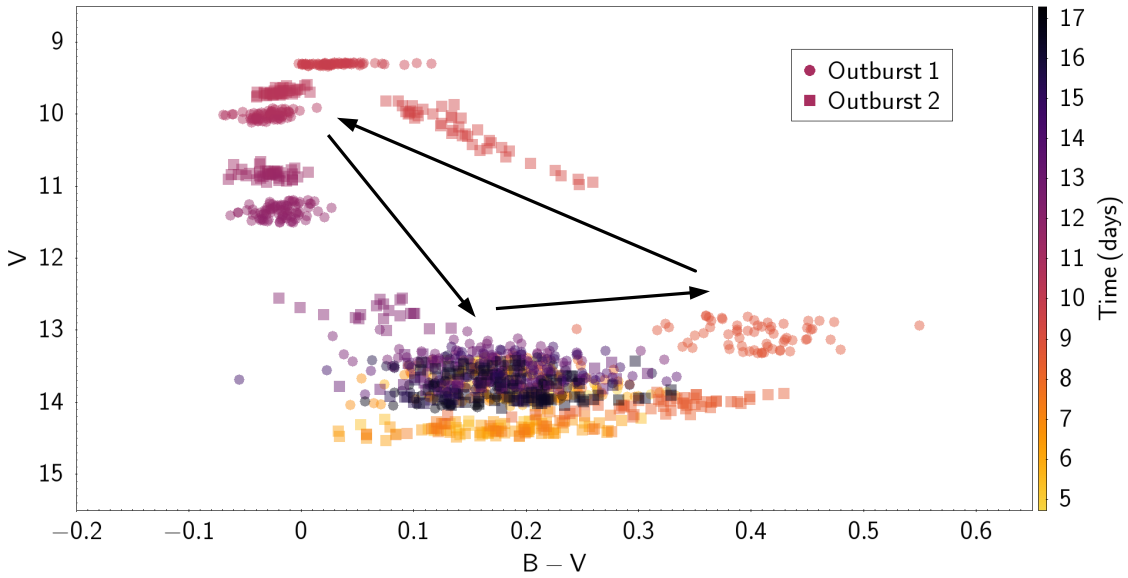

Fig. 4. Colour variations across an outburst of VW Hyi. The arrows show the direction of the time evolution in the diagram.

light, heating of the outer rim of the accretion disc as described in Buat-Ménard et al. (2001) is not taken into account. The inner disc may be truncated, either because the white dwarf is magnetised, in which case truncation occurs at the magnetospheric radius, or because of a transition to an optically thin flow occurring close to the white dwarf. In the latter case we assume the same dependence of the inner disc radius as a function of the mass accretion rate as in the magnetic case, thereby introducing an effective magnetic dipole moment μ. Observations indeed indicate that during quiescence the accretion disc does not reach the white dwarf surface (see e.g. Balman 2015; Baptista & Wojcikiewicz 2020, for recent references). We calculate the time-dependent effective temperature as a function of the radius, and we then generate disc spectra by summing ATLAS9 Kurucz ODFNEW/NOVER stellar atmosphere models (Castelli et al. 1997) from each disc ring. This library covers the ranges 3500 K $\leq T_{\rm eff} \leq$ 50 000 K and 0 $\leq \log g \leq 5$, $T_{\rm eff}$ being the effective temperature and g the surface gravity. We interpolate $F_\lambda/F_{\lambda,BB}$, where F_λ and $F_{\lambda,BB}$ are the flux provided by the library and the blackbody flux respectively. When $T_{\rm eff}$ or log g falls outside the tabulated values, we use the last available value of $F_\lambda/F_{\lambda,BB}$. We then estimate the *UBVR* magnitudes using the tabulated transmissions by Bessell (1990).

This way of calculating spectra does not take into account that in a disc gravity increases with altitude, nor that energy is dissipated in the atmosphere. When calculating the vertical profiles and the relation between the local effective temperature and surface density, we do however take into account energy dissipation throughout the disc, from the midplane up to the photosphere. One of the consequences of this approach is that a disc spectrum obtained by summing stellar spectra predicts strong Balmer jumps that are either not observed or are much weaker than predicted (La Dous 1989). Moreover, the strong emission lines observed during outbursts are also not

predicted by the models; these lines indicate the presence of optically thin emitting material, possibly in the form of a wind (see e.g. Matthews et al. 2015). But given that the energy dissipation in optically thin layers, despite recent progresses, is not well constrained, we refrain from using a more sophisticated treatment, as done for example by Wade & Hubeny (1998). We instead consider the two extreme cases of blackbodies and stellar spectra.

3.2. Irradiated secondary

The secondary is irradiated by the accretion luminosity; the irradiated side reaches a temperature given by

$$\sigma T_{2,\rm irr}^4 = \sigma T_2^4 + (1-\eta)\frac{1}{2}\frac{GM_1\dot{M}}{r_{\rm wd}}\frac{1}{4\pi a^2}, \quad (1)$$

where σ is the Stephan–Boltzman constant, T_2 the unirradiated temperature of the secondary, η the albedo, M_1 the white dwarf mass, $r_{\rm wd}$ its radius, $\dot{M}$ the accretion rate, and a the orbital separation. The factor 1/2 accounts for the fact that half of the accretion luminosity is emitted by the boundary layer in the EUV domain that is not able to penetrate deep in the atmosphere of the secondary, and is thus inefficient for raising its temperature.

The contribution of the secondary is then taken to be the average of the illuminated and unilluminated spectra, that we model as blackbodies. Given the oversimplified treatment of the variation of the effective temperature over the stellar surface, using accurate stellar spectra is not required.

3.3. White dwarf

The white dwarf spectrum is taken from Levenhagen et al. (2017) who provides theoretical spectra for hot DA white dwarfs with effective temperatures in the range 17 000 K–100 000 K, and $7 \leq \log g \leq 9.5$. We also assume that the white-dwarf temperature remains constant during the outburst cycle. We expect that the white dwarf should be hotter at the end of an outburst than at its onset. Godon et al. (2017) reported a decrease in the white dwarf temperature in U Gem from 41 500 K to 36 250 K after a long (two weeks) outburst. This effect is observed and expected (Piro et al. 2005) to be significant only for long duration outbursts, and we do not take it into account here.

3.4. Hot spot

The hot spot luminosity is taken as (Smak 2002)

$$L_{\rm hs} = \frac{1}{2}\frac{G(M_1+M_2)\dot{M}_{\rm tr}}{a}\Delta v^2, \quad (2)$$

where $\dot{M}_{\rm tr}$ is the mass transfer rate from the secondary, M_2 is the secondary mass, and Δv^2 is a dimensionless quantity of order unity that depends on the degree of the disc's Roche-lobe filling and, more weakly, on the mass ratio. A fit to Δv^2 is given by Smak (2002). We ignore the possibility that the stream overflows the accretion disc. Stream overflow slightly modifies the outburst cycle, but this is a limited effect that can easily be compensated for by changes in the mass transfer rate or in the viscosity parameter. More importantly, it changes the luminosity due to the incorporation of matter at smaller radii as well as the colour temperature of this contribution in a non-trivial way; however, it is likely that both the luminosity and effective temperature would be higher than estimated here.

Observations indicate hot spot temperatures in the range 10^4–1.5×10^4 K (see e.g. Bruch et al. 2000, and references therein). For consistency with Schreiber et al. (2003), we assume a blackbody spectrum with a temperature of 10^4 K, which is more appropriate for SS Cyg because of its long orbital period. This probably overestimates the contribution of the hot spot in the B and V bands, but, as we see later, this contribution is by far not dominant and our results are relatively insensitive to the precise temperature of the hot spot.

Table 1. Model parameters.

System	SS Cyg	VW Hyi
$P_{\rm orb}$ (h)	6.60	1.78
M_1 ($M_\odot$)	1.00	0.70
M_2 ($M_\odot$)	0.67	0.10
$\cos i$	0.7	0.7
$\dot{M}_{\rm tr}$ (10^{16} g s^{-1})	15	0.8
$T_{\rm wd}$ (K)	50 000	20 000
T_2 (K)	4200	3200
η	0.8	0.9
d (pc)	114	54
$\alpha_{\rm c}$	0.02	0.04
$\alpha_{\rm h}$	0.1	0.2

4. Results

4.1. SS Cyg

The parameters we use in the case of SS Cyg are given in Table 1. The distance is from *Gaia* DR2 (Gaia Collaboration 2016, 2018). We choose the primary mass $M_1 = 1\,M_\odot$ for the same reasons as discussed in Hameury et al. (2017), in line with the recent determination by Hill et al. (2017), and take the mass ratio $q = M_2/M_1$ from Bitner et al. (2007). From an analysis of the ellipsoidal variations, Bitner et al. (2007) limit the inclination to the range $45° < i < 56°$, in line with the absence of eclipses and the presence of orbital humps; we adopt here $i = 45°$. The effective temperature we use (4200 K) is lower than the temperature corresponding to the observed spectral type of the secondary (K4V – K5V), but the secondary is highly spotted (Webb et al. 2002), and this low temperature is needed to fit the observed visual magnitude during quiescence. We could have used a temperature of 4500 K corresponding to a K5 dwarf, with a surface reduced by 19% due to the presence of dark spots that would have given the same V magnitude for the secondary, with a $B-V$ reduced by 0.11 mag. Given the dilution of the secondary light, the change in $B-V$ during quiescence would be only 0.05 mag; both options therefore give essentially identical results. It should also be noted that the luminosity of the secondary deduced by Bitner et al. (2007) is compatible only with a distance larger that 140 pc (R. Robinson, priv. comm.), which we now know to be contrary to observations. The white dwarf temperature is taken from Sion et al. (2010).

We use $\alpha_{\rm h} = 0.1$ on the hot branch, and $\alpha_{\rm c} = 0.02$ in the cold state. The mass transfer rate was set to 2×10^{17} g s^{-1}, so that the average recurrence time is 48 days when the disc is not truncated. When the disc extends to the white dwarf surface, the light curve, shown in Fig. 5 consists of a sequence of alternating long (about 30 days) and short (15 days) outbursts, during which respectively 41% and 9% of the total disc mass is accreted. These outbursts are significantly longer than those observed, but, as we show later in this section, the colour evolution is about the same in both cases. We also consider the case where the disc is

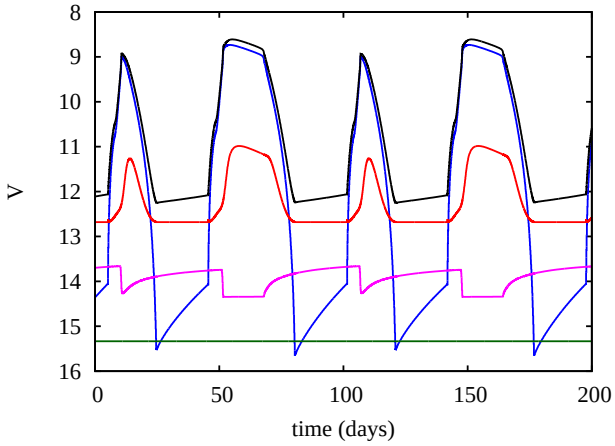

Fig. 5. Luminosity variations in the V band of each component in SS Cyg in the case where the inner disc is not truncated. Shown are curves representing the accretion disc (blue), the contribution from the secondary (red), the contribution from the hot spot (magenta), and the constant light from the white dwarf (green). The total optical luminosity is shown in black.

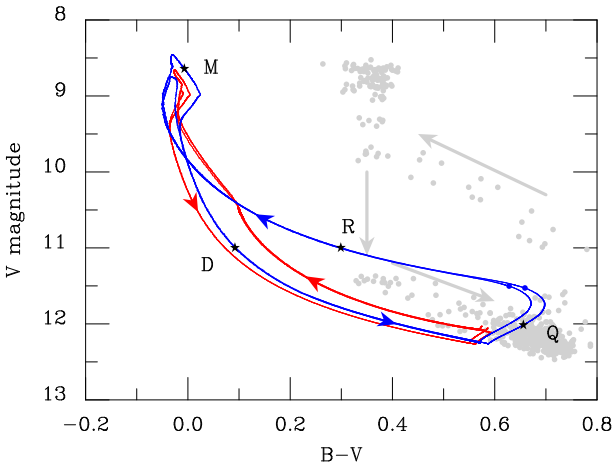

Fig. 6. Colour variations predicted by the model for parameters corresponding to SS Cyg. Shown is the case where the inner disc is truncated (in blue), and when it extends down to the white dwarf surface (in red). For the sake of clarity, $B-V$ has been increased by 0.02 mag in the truncated case, so that the blue and red curves do not superimpose during decay. The arrows indicate the direction of the time evolution. The dots at $V \sim 11.5$ indicate the onset of the outburst in the truncated case. The differences between the short and long outbursts are visible, but small. The stars denote the positions at which spectra are shown in Fig. 7, and the grey dots are the observational data points.

truncated; we use a magnetic moment $\mu = 2\times10^{30}$ G cm^3, corresponding to an inner radius of 2.2×10^9 cm in quiescence, about 4 times the white dwarf radius. The outbursts are also bimodal and have similar properties, except that the recurrence time is twice as long.

Figure 5 also shows the contribution of each component of the system to the total light curve. During quiescence, most of the optical light originates from the secondary, with some contribution from the hot spot. During outbursts the disc dominates, with a small contribution from the irradiated secondary; the decrease in the hot spot luminosity during outbursts results from the disc expansion.

Figure 6 shows the colour variations predicted by the model. There is a clear hysteresis in both cases. We first consider the case where the disc is not truncated. At the end of an outburst the

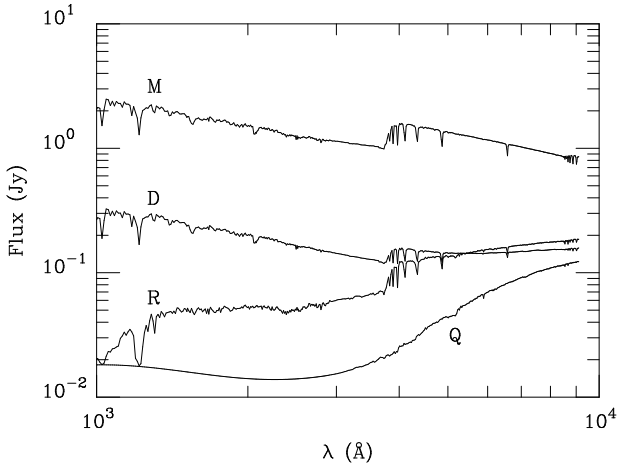

Fig. 7. Spectral evolution during an outburst of SS Cyg: quiescence (Q), rise (R), plateau (M), and decay (D). The corresponding locations in the colour–magnitude diagram are indicated in Fig. 6.

V magnitude is at a minimum; during quiescence the luminosity slowly rises, and the system becomes redder because, although the disc effective temperature increases, it is comparable to the secondary temperature and much lower than the hot spot temperature which provides a significant fraction of the luminosity in the B band. At some point, an instability is triggered in the inner disc, and the effective temperatures becomes higher than 10^4 K, so that the system become bluer and brighter. When the system is close to its maximum, the colour remains roughly constant, with a (limited) variation pattern that is rather complex. During decay the system initially evolves at a constant $B-V$, while the disc is fully in the hot state, and then becomes bluer and fainter while a cooling front propagates, bringing the outer part of the disc to temperatures low enough that they do not contribute any longer to the total luminosity, while the innermost-disc luminosity and temperatures keep increasing for a while; during the final decay the disc temperatures decrease everywhere, and the system gets fainter and reddens until the disc is fully brought to the cool state and the luminosity is at its minimum.

The fundamental reason for the colour difference at a given magnitude between rise and decay is that the disc is less massive during decay than during rise, and that the mass distribution with radius is also quite different; when the eruption starts, the surface density Σ approximately follows the critical surface density profile, and increases with radius, while the effective temperature is roughly constant. On the other hand, just after maximum, the disc is not far from steady state, and Σ and $T_{\rm eff}$ typically decrease as $r^{-3/4}$. This is the same reason that explains the hysteresis of SS Cyg in a diagram combining optical, X-rays, and EUV fluxes (Hameury et al. 2017).

The evolution of a disc truncated in quiescence is similar, except that the luminosity and colour variations in quiescence are more important than in the non-truncated case because, as a result of truncation, the disc is allowed to be brighter and represents a larger faction of the total luminosity (in quiescence the accretion rate strongly increases with radius). The colour evolution in quiescence is initially the same as in the non-truncated case: the system reddens, until the effective temperature of the inner disc becomes comparable to that of the secondary (the maximum effective temperature for the disc to stay on the cold branch is 5800 K), at which point $B-V$ decreases.

It is interesting to note that the evolution in the colour–magnitude diagram is almost the same for short and long

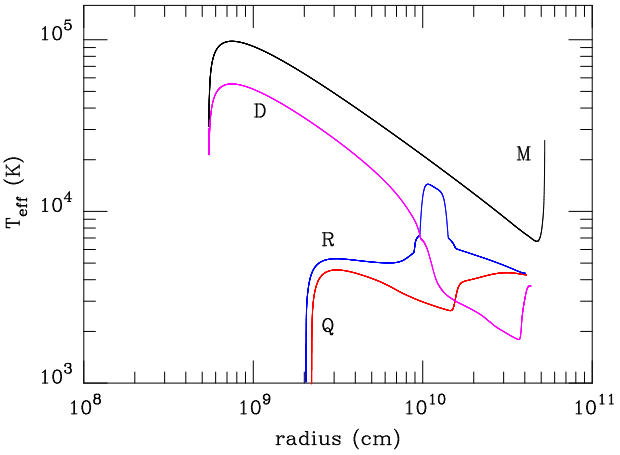

Fig. 8. Radial profiles of the disc effective temperature at the four epochs shown in Fig. 7.

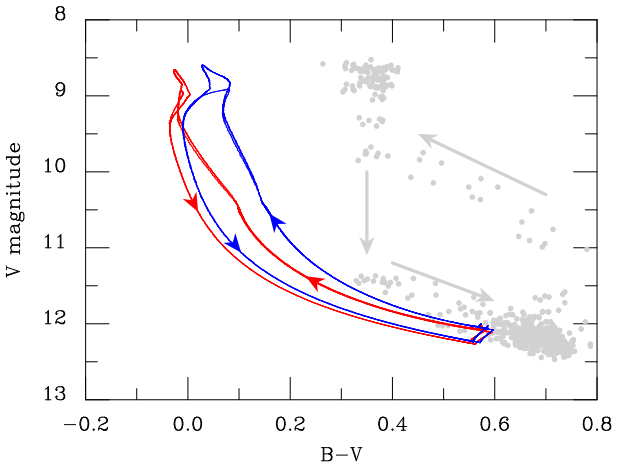

Fig. 9. Same as Fig. 6, but for the disc spectrum calculated using stellar spectra (red curve) or blackbodies (blue curve). In both cases, the disc is not truncated.

outbursts. This occurs because the heat front is able to reach the outer disc edge in both cases, and matter redistribution in the disc is efficient even for short outbursts.

Figure 7 shows the spectral evolution of the modelled system during a large outburst when the disc is truncated. In quiescence, the red part of the spectrum is dominated by the secondary, while the hot spot is responsible for the observed light in the blue and UV domain; the accretion disc is essentially not detectable. The spectra calculated during the rise and decay are very different, although the visual magnitude is the same (11.0) for both spectra; in both cases the disc dominates, but during rise the total spectrum resembles that observed during quiescence. This is so because during rise the mass distribution in the disc is very similar to that in quiescence, whereas during decay the mass distribution, the effective temperature, and hence the disc spectrum are close to those of a steady disc; the spectrum during decay is essentially the same as at maximum. This is clearly illustrated in Fig. 8, which shows the radial dependence of the disc effective temperature. In quiescence, the effective temperature does not vary much with radius, and is of the order of 3000−4000 K. The spectrum labelled "R" corresponds to the case where two heating fronts are propagating in the disc; the portion 1.0×10^{10} cm $< r < 1.4 \times 10^{10}$ cm is on the hot branch, whereas the temperatures of innermost and outermost portions of

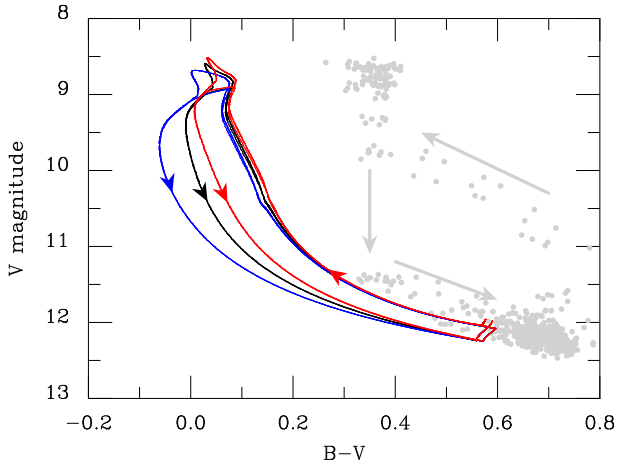

Fig. 10. Same as Fig. 6, but for different values of the albedo: 1.0 (blue curve), 0.8 (black curve), and 0.6 (red curve). In all three cases, the disc in not truncated and the spectra are calculated using blackbodies.

the disc are those of quiescence. At maximum the disc is close to being steady; the rise in $T_{\rm eff}$ at the disc edge is due to tidal dissipation, which is important because the disc has reached the tidal truncation radius. During decay the outer portion of the disc is brought on the cold branch, which is cooler than during rise because mass has been transferred to the inner disc; these inner portions are still on the hot branch, with $T_{\rm eff}$ close to a steady profile.

The colour–magnitude diagram significantly depends on the assumptions made when calculating the disc spectrum. Figure 9 compares the colour–magnitude diagrams obtained when assuming that the spectrum calculated at a given radius is a blackbody (blue curve) or a stellar spectrum (red curve). Whereas the decay phase is relatively independent of the assumption made, the system is, for a given optical magnitude, redder when we assume blackbody spectra. This occurs because the Balmer jump during decay is small, so that the local disc spectrum is, in the visible domain, close to that of a blackbody, whereas the jump is large during the rising part; when $V = 10$, the Balmer jump is about 0.86 mag if the system rises, and 0.43 if it is declining. This is consistent with observations that show that the Balmer jump is stronger during rise than decline, but as was already noted by La Dous (1989), the jump is stronger than observed, in particular during the declining part where the jump is observed to be almost zero. La Dous (1989) concluded that energy dissipation in the atmosphere, not accounted for in Kurucz stellar models, must be significant.

Figure 10 illustrates the influence of the secondary irradiation on the colour–magnitude diagram. Irradiation produces additional light that reddens the spectrum emitted by the disc and white dwarf alone; we considered three possible values for the albedo: 1.0 (no irradiation), 0.8 (our reference value), and 0.6 (large irradiation effect). As can be seen, $B - V$ increases with decreasing albedo, as expected. We also note that the rise is not much affected by irradiation, whereas the effect is quite significant during the decay phase. This occurs because, for a given optical magnitude, the mass accretion rate onto the white dwarf is much higher during the decay than during the rise; as an example, for $V = 10$, $\dot{M}$ is 5.6×10^{16} g s^{-1} during rise and 3.8×10^{18} g s^{-1} during decay.

When compared to observed outbursts, we note that the quiescence and outburst magnitudes agree well with observations, which should not come as a surprise because the model

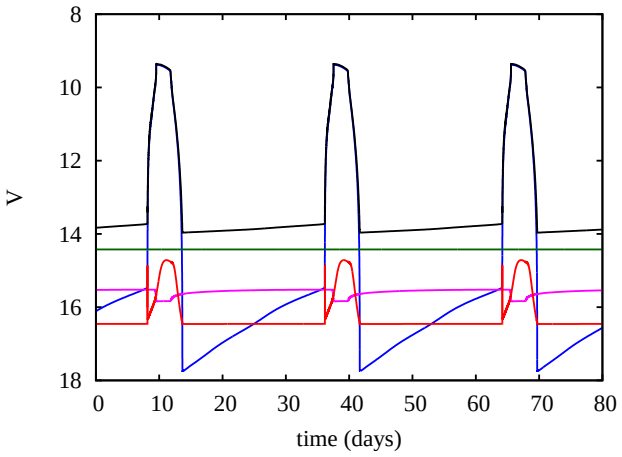

Fig. 11. Same as Fig. 5, but for parameters corresponding to VW Hyi.

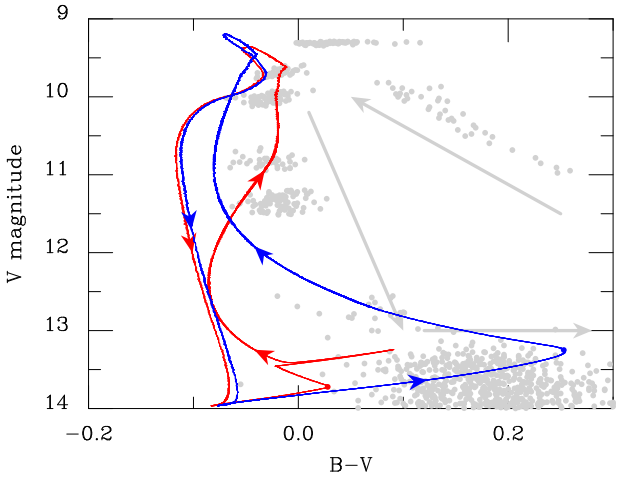

Fig. 12. Same as Fig. 6, but for parameters corresponding to VW Hyi. In the case of disc truncation, the track followed by VW Hyi has been shifted to the left by 0.005 mag.

parameters were chosen to assure just that. The colour during quiescence also agrees reasonably well with observations, and with the general evolution scheme. The amplitude of the hysteresis (a difference of 0.2 mag at $V = 11$) is not grossly different – but significantly smaller – from what is observed (0.4 mag). On the other hand, the system is too blue at outburst maximum by about 0.4 mag. This discrepancy probably has the same root cause as the smaller-than-observed amplitude of the hysteresis cycle. Given that at maximum more than 90% of the optical light is emitted by the disc, and that the disc is close to being steady, the disc spectrum at maximum is not very sensitive to the model parameters. We anticipate, however, that explaining the observed behaviour in U will not be straightforward as the observed colour evolution is extremely different when considering $B - V$ and $U - B$, whereas we expected a relatively similar behaviour.

4.2. VW Hyi

The parameters for VW Hyi are given in Table 1. The distance is from *Gaia* DR2 (Gaia Collaboration 2016, 2018). The primary and secondary masses are rather uncertain; Smith et al. (2006) quote a primary mass of $0.71^{+0.18}_{-0.26}\,M_\odot$ based on radial velocities, while Long et al. (2009) determine a mass of $0.93\,M_\odot$ based on spectral fitting of the white dwarf emission. The latter determination is based on a distance of 65 pc, and Long et al. (2009) noted it should be revised to lower masses for larger distances, with $0.71\,M_\odot$ for a distance of 74 pc. Given the *Gaia* distance, this would imply a mass close to $1\,M_\odot$. Here we chose to use the spectroscopic determination of the masses, $M_1 = 0.7\,M_\odot$. The secondary mass is then estimated from the mass ratio $q = 0.147 \pm 0.05$ found by Patterson et al. (2005) from the superhump period. The white dwarf temperature is found to vary between 24 000 K at the end of a superoutburst to 20 000 K before the next outburst. We use here $T_2 = 20\,000$ K. The secondary spectral type is mid to late M (Hamilton et al. 2011); we adopt here a secondary temperature of 3200 K.

We use $\alpha_{\rm h} = 0.2$ on the hot branch, and $\alpha_{\rm c} = 0.04$ in the cold state; these values are twice as high as those used for SS Cyg, but the ratio of the two is the same. With a mass transfer rate of $8 \times 10^{15}\,{\rm g\,s^{-1}}$, we obtain outbursts lasting for 5 d and recurring every 28 d when the disc is not truncated. When the disc is truncated with an inner disc radius of 1.8×10^9 cm during quiescence, that is 2.3 times the white dwarf radius ($\mu = 10^{30}\,{\rm G\,cm^3}$), these numbers are 6 d and 50 d, respectively. The light curve is shown in Fig. 11, together with the contributions from the various components of the system. There are significant differences with SS Cyg. First, the smaller disc size results in shorter outbursts cycles, both in terms of outburst duration and recurrence times; the latter varies as the square root of the outer disc radius (Lasota 2001), while the outburst duration depends on the disc size and on the mass transfer rate. In addition, the quiescence luminosity is dominated by the white dwarf that represents almost 2/3 of the visual luminosity, with a significant contribution from the hot spot and, to a lesser extent, from the secondary and the disc that becomes the second contributor just prior to an outburst. We also note a sharp increase in the secondary luminosity at the onset of an outburst, which is caused by a sharp peak in the accretion rate occurring when the inner heating front reaches the white dwarf surface. This peak lasts for less than a minute, and is not physical.

Figure 12 shows the corresponding colour–magnitude diagram. The main differences with SS Cyg is that VW Hyi is much bluer because the secondary's contribution is much smaller. The spike that appears at $V \sim 13.5$ in the non-truncated case is due to the peak in the accretion rate when the heating front reaches the inner disc edge.

As in the case of SS Cyg, the predicted magnitudes agree well with observations; the amplitude of the colour difference between rise and decay is slightly smaller than what is observed, even though the decay is slightly bluer than observed (typically 0.1–0.2 mag); as mentioned above, this is presumably due to our inability to accurately model the disc spectrum, even when the disc is steady. However, the model does not reproduce the reddening observed during the initial rise (the system is expected to redden during quiescence, but as soon as it enters into outburst, it becomes bluer). La Dous (1994) suggested that this initial reddening occurs because the outburst is initiated in the outer disc and that, even on the hot branch, the outer disc is too cool to contribute significantly in the UV and, to a lesser extent, in the blue. For a system such as VW Hyi where the main contributor to the B and V bands is a hot white dwarf, this could in principle be a possibility; the effective temperature is of the order of $1.2 \times 10^4 r_{10}^{-3/4}\,\dot{M}_{17}^{1/4}$ K for the parameters of VW Hyi, r_{10} being the radius in units of 10^{10} cm and $\dot{M}_{17}$ the local accretion rate in units of $10^{17}\,{\rm g\,s^{-1}}$, so that the additional contribution of a ring entering the hot state would be redder than the white dwarf. The

main problem with this interpretation is that we were not able to find reasonable parameters for which outbursts of the outside-in type would be triggered unless it were due to mass-transfer enhancement not giving rise to a superoutburst, which would require some fine-tuning of the parameters.

5. Conclusion

Observations show that dwarf novae follow a characteristic loop in the $(B-V, V)$ colour–magnitude diagram. Its overall properties can be accounted for by the DIM, with some deficiencies, however.

The agreement with observations during quiescence is very good, which might come as a surprise since modelling the disc spectra is notoriously difficult at low accretion rates. This is the result of the disc being extremely faint in quiescence for the two systems that we consider here: the main contributor to the optical light is the secondary star in the case of SS Cyg, and the primary for VW Hyi.

The evolution of a system in the colour–magnitude diagram is affected by the spectral modelling of the accretion disc for the raising part of the outburst, and by the magnitude of irradiation during the decay. Disc spectra are not well approximated by a summation of stellar spectra because of energy dissipation in the disc atmosphere. As mentioned earlier, attempts to take this effect into account used simple prescriptions for the local dissipation rate (e.g. Shaviv & Wehrse 1986; Kriz & Hubeny 1986; Wade & Hubeny 1998) that might not be a good description of reality. In addition, our synthetic spectra show absorption lines, and the observed emission lines that must be produced in hot optically thin regions cannot be reproduced by our model nor by any of the above-mentioned disc models. In principle, the coupling of MRI simulations with a radiative transfer model should enable us to calculate properly the spectra of accretion discs; however, MRI models still have difficulties in reproducing the values of α needed to account for the general timing properties of dwarf novae, making such a development of little interest for the time being.

We did not consider here the U band because the effect of the Balmer jump will be even stronger than in the B band. We calculated the predicted $(U-B, V)$ colour–magnitude diagrams; they are very similar to the $(B-V, V)$ diagrams, with $U-B=0.4$ in quiescence and -0.6 in outburst in the case of SS Cyg. This is quite different from the values given by Bailey (1980) who finds that $B-V$ is identical in quiescence and at maximum. This is certainly due in part to our poor modelling of the disc spectrum, but also perhaps to the presence of hot and optically thin gas that radiates in the UV.

In summary, the DIM can explain the existence and orientation of this hysteresis, which is a direct consequence of the total mass variation of the accretion disc and of the differences in the mass radial distribution in the accretion disc between raise and decay. It can also explain the approximate colour and magnitude ranges covered during the evolution. On the other hand, the DIM cannot explain the "redder than observed" colours near the peak of the outbursts, and the observed U-band behaviour; these are the same problems that have plagued spectral discs models for a long time, and that reflect our inability to model even steady-state discs correctly.

Acknowledgements. We acknowledge with thanks the variable star observations from the AAVSO International Database contributed by observers worldwide and used in this research. This work was supported by a National Science Centre, Poland grant 2015/19/B/ST9/01099. JPL was supported by a grant from the French Space Agency CNES. This work has made use of data from the European Space Agency (ESA) mission *Gaia* (https://www.cosmos.esa.int/gaia), processed by the *Gaia* Data Processing and Analysis Consortium (DPAC, https://www.cosmos.esa.int/web/gaia/dpac/consortium). Funding for the DPAC has been provided by national institutions, in particular the institutions participating in the *Gaia* Multilateral Agreement.

References

Bailey, J. 1980, MNRAS, 190, 119
Balbus, S. A., & Hawley, J. F. 1991, ApJ, 376, 214
Balman, S. 2015, Acta Polytech. CTU Proc., 2, 116
Baptista, R. 2016, in Astronomy at High Angular Resolution, eds. H. M. J. Boffin, G. Hussain, J. P. Berger, & L. Schmidtobreick, 439, 155
Baptista, R., & Wojcikiewicz, E. 2020, MNRAS, 492, 1154
Bath, G. T., & van Paradijs, J. 1983, Nature, 305, 33
Bessell, M. S. 1990, PASP, 102, 1181
Bitner, M. A., Robinson, E. L., & Behr, B. B. 2007, ApJ, 662, 564
Bruch, A., Steiner, J. E., & Gneiding, C. D. 2000, PASP, 112, 237
Buat-Ménard, V., & Hameury, J. M. 2002, A&A, 386, 891
Buat-Ménard, V., Hameury, J.-M., & Lasota, J.-P. 2001, A&A, 366, 612
Cannizzo, J. K. 2012, ApJ, 757, 174
Cannizzo, J. K., & Kenyon, S. J. 1987, ApJ, 320, 319
Castelli, F., Gratton, R. G., & Kurucz, R. L. 1997, A&A, 318, 841
Coleman, M. S. B., Kotko, I., Blaes, O., Lasota, J. P., & Hirose, S. 2016, MNRAS, 462, 3710
Gaia Collaboration (Prusti, T., et al.) 2016, A&A, 595, A1
Gaia Collaboration (Brown, A. G. A., et al.) 2018, A&A, 616, A1
Godon, P., Shara, M. M., Sion, E. M., & Zurek, D. 2017, ApJ, 850, 146
Hambsch, F. J. 2019, Observations from the AAVSO International Database, https://www.aavso.org
Hameury, J.-M. 2019, Adv. Space Res., submitted [arXiv:1910.01852]
Hameury, J.-M., Menou, K., Dubus, G., Lasota, J.-P., & Hure, J.-M. 1998, MNRAS, 298, 1048
Hameury, J.-M., Lasota, J.-P., & Warner, B. 2000, A&A, 353, 244
Hameury, J. M., Lasota, J. P., Knigge, C., & Körding, E. G. 2017, A&A, 600, A95
Hamilton, R. T., Harrison, T. E., Tappert, C., & Howell, S. B. 2011, ApJ, 728, 16
Hill, C. A., Smith, R. C., Hebb, L., & Szkody, P. 2017, MNRAS, 472, 2937
Horne, K. 1985, MNRAS, 213, 129
Horne, K., & Cook, M. C. 1985, MNRAS, 214, 307
Hubeny, I. 1990, ApJ, 351, 632
Idan, I., Lasota, J.-P., Hameury, J.-M., & Shaviv, G. 2010, A&A, 519, A117
Knigge, C., Long, K. S., Blair, W. P., & Wade, R. A. 1997, ApJ, 476, 291
Knigge, C., Long, K. S., Wade, R. A., et al. 1998, ApJ, 499, 414
Körding, E., Rupen, M., Knigge, C., et al. 2008, Science, 320, 1318
Kriz, S., & Hubeny, I. 1986, Bull. Astron. Inst. Czechoslov., 37, 129
La Dous, C. 1989, MNRAS, 238, 935
La Dous, C. 1994, Space Sci. Rev., 67, 1
Lasota, J.-P. 2001, New Astron. Rev., 45, 449
Levenhagen, R. S., Diaz, M. P., Coelho, P. R. T., & Hubeny, I. 2017, ApJS, 231, 1
Long, K. S., Gänsicke, B. T., Knigge, C., Froning, C. S., & Monard, B. 2009, ApJ, 697, 1512
Matthews, J. H., Knigge, C., Long, K. S., Sim, S. A., & Higginbottom, N. 2015, MNRAS, 450, 3331
Nixon, C. J., & Pringle, J. E. 2019, A&A, 628, A121
Osaki, Y. 1989, PASJ, 41, 1005
Patterson, J., Kemp, J., Harvey, D. A., et al. 2005, PASP, 117, 1204
Piro, A. L., Arras, P., & Bildsten, L. 2005, ApJ, 628, 401
Puebla, R. E., Diaz, M. P., & Hubeny, I. 2007, AJ, 134, 1923
Roberts, J. 2019, Observations from the AAVSO International Database, https://www.aavso.org
Scepi, N., Lesur, G., Dubus, G., & Flock, M. 2018, A&A, 609, A77
Schreiber, M. R., Hameury, J.-M., & Lasota, J.-P. 2003, A&A, 410, 239
Shakura, N. I., & Sunyaev, R. A. 1973, A&A, 500, 33
Shaviv, G., & Wehrse, R. 1986, A&A, 159, L5
Sion, E. M., Godon, P., Myzcka, J., & Blair, W. P. 2010, ApJ, 716, L157
Smak, J. 1994, Acta Astron., 44, 265
Smak, J. 2002, Acta Astron., 52, 263
Smak, J. 2009, Acta Astron., 59, 121
Smith, A. J., Haswell, C. A., & Hynes, R. I. 2006, MNRAS, 369, 1537
Wade, R. A. 1984, MNRAS, 208, 381
Wade, R. A. 1988, ApJ, 335, 394
Wade, R. A., & Hubeny, I. 1998, ApJ, 509, 350
Warner, B. 2003, Cataclysmic Variable Stars (Cambridge: Cambridge University Press), 592
Webb, N. A., Naylor, T., & Jeffries, R. D. 2002, ApJ, 568, L45
Yi, I., & Kenyon, S. J. 1997, ApJ, 477, 379